Reinforced concrete plates: cracking and ultimate load through Lumped Damage Mechanics

Rafael N. Cunha[1], David L.N.F. Amorim[1,2,3], Sergio P.B. Proença[3], Julio Flórez-López[4]

[1]*Graduate Program of Civil Engineering, Federal University of Alagoas*
Av. Lourival Melo Mota s/n, Tabuleiro do Martins, Maceió, 57072-970, Alagoas, Brazil
rafael.cunha@ctec.ufal.br
[2]*Disaster Research Institute, Federal University of Sergipe*
Av. Marcelo Deda Chagas s/n, Rosa Elze, São Cristóvão, 49107-230, Sergipe, Brazil
davidnf@academico.ufs.br
[3]*Graduate Program of Civil Engineering, São Carlos School of Engineering, University of São Paulo*
Av. Trabalhador são-carlense 400, Pq. Arnold Schimidt, São Carlos, 13566-590, São Paulo, Brazil
persival@sc.usp.br
[4]*School of Civil Engineering, Chongqing University*
Shapingba-District, 400045, Chongqing, China
j.florezlopez@cqu.edu.cn

Abstract. The present paper proposes a new finite element formulation for the analysis of RC slabs, accounting for concrete cracking and reinforcement yielding. The proposed formulation, developed within the framework of Lumped Damage Mechanics, considers that all inelastic effects are localized in lines and relates all numerical parameters to the mechanical properties of the slab. The proposed variational approach is presented as a Nash non-cooperative equilibrium point. It is verified, numerically, that the proposed FE leads to mesh-independent results. Numerical simulations of some experimental tests are also presented. The results in terms of collapse mechanism, cracking network, and force-deflection curves showed that the model has significant accuracy, even for non-symmetric free clamped and simple supported boundary conditions. It is also shown, through the confrontation with experimental results, that the model correctly characterizes the initiation and development of complex networks of cracks.

Keywords: Nonlinear analysis; Reinforced concrete slabs; Lumped Damage Mechanics; Cracking pattern.

1 Introduction

The cracking process of Reinforced Concrete (RC) slabs have been studied since the early 20th century. The first approaches were presented by applying the theory of plasticity, in the limit analysis, aiming to get the collapse loads of slabs, by estimating the collapse mechanism. These studies led to the development of the yield line theory (YLT).

The YLT was firstly presented by Bach [1], but for a few numbers of slabs, based on the upper-bound theorem [2]. Later the YLT was expanded by Ingerslev [3], for simple supported rectangular slabs, and finally presented in a formal way by Johansen [4]. The concept of hinge line was also presented, which physically defines the rupture lines in the slabs and mathematically, the concepts of plastic hinges of the theory of plasticity. This theory was expanded to cover more cases [5, 6].

The studies of RC slabs were also made in the experimental field, by extensive campaigns, which several RC slabs were molded and collapsed, which bearing capacities were compared to the one obtained by the YLT, as the ones presented by [6, 7].

The use of the finite element method allowed the development of more complex studies, by applying different theories to describe the cracking and damage process, as by continuum damage [8], extended finite element [9] or smeared crack [10] approaches.

Other approach to analyses the nonlinear effects of structures are the Lumped Damage Mechanics. This theory was presented in the early nineties for the analysis of RC frames under seismic loads [11–15] and expanded for continuum media [16–18] and RC slabs [19]. Note that this theory already showed mesh-independence [17,

19, 20].

Therefore, the objective of this paper is presenting a comparative analysis on RC concrete slabs analyzed by using the LDM theory, the YLT and experimental results. Slabs with different geometries and boundary conditions were compared in terms of damage distribution with experimental cracking pattern and bearing capacity with the plastic hinge theory. It is observed that the results by using the LDM presented great accuracy, even for complex cracking networks, and the collapse loads were quite close to the YLT, in favor of safety.

2 Yield Line Theory

The yield line theory presents three main hypotheses: the rupture lines (hinge lines) are straight lines; the slab collapse mechanism is characterized by hinge lines, and the parts enclosed remain flat; along the hinge line, the bending moment is equal to the bearing moment of the slab. The analysis of slabs may be made by the segment equilibrium or by the virtual work method. This paper is focused on the last method.

Consider a slab under a concentrated load P in its center. The bending moments and the loads are in equilibrium, when the yield lines are formed. The virtual work method states that the external work made by the loads to create a virtual deflection must be equal to the virtual work done as the slab rotates at the yield lines to accommodate the deflection. Note that the elastic rotations and deflections are smaller than the ones by the plastic deformations, thus, they are not computed to the work equations [2]. For the case of a concentrated load in the center of the slab, the external work W_e for a unitary virtual deflection is given by:

$$W_e = P \times 1 \tag{1}$$

Considering the hypothesis that along the hinge line the bending moment is constant, the internal work of a slab may be computed by the product of the bending moment m, the length of the hinge line L and the rotation of the hinge line θ, for the unitary virtual deflection. In case of "*j*" hinge lines, the internal work W_i is computed as:

$$W_i = \sum_{n=1}^{j} m_n \times \theta_n \times L_n \tag{2}$$

Therefore, it is possible to define the bearing capacity of the slab, by equating the internal and external works.

3 Lumped damage modeling for reinforced concrete slabs

3.1 Constant Moment Triangle

Consider the constant moment triangle (CMT) plate finite element, presented by Morley [21], which have six degrees of freedom, being the deflection in the corners and the normal rotation in the middle side nodes, as presented in Fig. 1(a). The vector with the nodal deflections is written as:

$$\{U\} = \left\{ \begin{array}{cccccc} w_i & w_j & w_k & \theta_a & \theta_b & \theta_c \end{array} \right\} \tag{3}$$

being w_i, w_j, w_k, the deflections of the nodes *i, j, k*, respectively, θ_a, θ_b and θ_c, the normal rotations of the midside nodes, respectively.

Note that, it is possible to define the normal rotation to each side, ϕ_{ij}, ϕ_{jk}, and ϕ_{ki}, as the kinematic variable for the CMT. Therewith, the kinematic equation is rewritten as:

$$\{\phi\} = [B]\,\{U\} \tag{4}$$

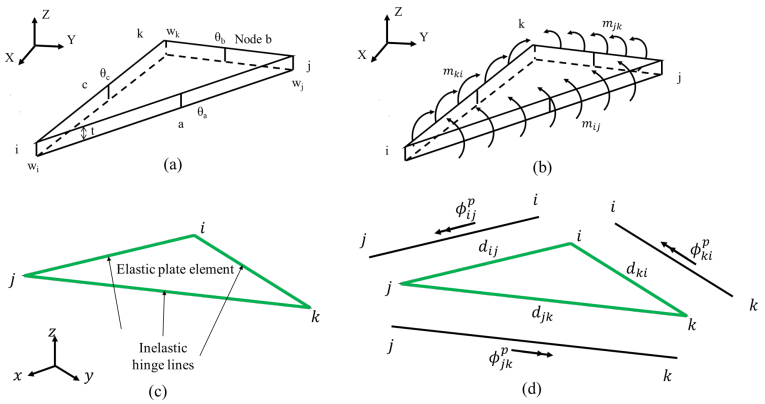

Figure 1. CMT plate element: (a) Degrees of freedom, (b) bending moments, (c) LDM considerations and (d) inelastic effects

$$[B] = \begin{bmatrix} \frac{c_{ij}(y_k-y_j)+s_{ij}(x_j-x_k)}{2A} & \frac{c_{ij}(y_i-y_k)+s_{ij}(x_k-x_i)}{2A} & \frac{L_{ij}}{2A} & 1 & 0 & 0 \\ \frac{L_{jk}}{2A} & \frac{c_{jk}(y_i-y_k)+s_{jk}(x_k-x_i)}{2A} & \frac{c_{jk}(y_j-y_i)+s_{jk}(x_i-x_j)}{2A} & 0 & 1 & 0 \\ \frac{c_{ki}(y_k-y_j)+s_{ki}(x_j-x_k)}{2A} & \frac{L_{ki}}{2A} & \frac{c_{ki}(y_j-y_i)+s_{ki}(x_i-x_j)}{2A} & 0 & 0 & 1 \end{bmatrix} \tag{5}$$

being x_i, x_j and x_k and y_i, y_j and y_k the coordinates of the nodes *i*, *j* and *k*, respectively. The L_{ij}, c_{ij} and s_{ij} are the length, cosine and sine of the side *ij*, respectively, and so for the other sides. A is the area of the plate element.

Conjugated to the normal rotations, the normal bending moments (Fig. 1(b)) is given:

$$\{M\} = \begin{Bmatrix} L_{ij}m_{ij} & L_{jk}m_{jk} & L_{ki}m_{ki} \end{Bmatrix} \tag{6}$$

where m_{ij} is the bending moment of the side *ij*, as shown in Fig. 1(b), and so for the other sides. The elasticity law may be defined according to Eq. 7:

$$\{\Phi\} = [F_0]\{M\} \rightarrow [F_0] = A[T][D][T] \tag{7}$$

being:

$$[D] = \frac{Et^3}{12(1-\nu^2)} \begin{bmatrix} 1 & \nu & 0 \\ \nu & 1 & 0 \\ 0 & 0 & \frac{1-\nu}{2} \end{bmatrix} \tag{8}$$

$$[T] = \begin{bmatrix} -L_{ij}c_{ij}^2 & -L_{ij}s_{ij}^2 & -2L_{ij}c_{ij}s_{ij} \\ -L_{jk}c_{jk}^2 & -L_{jk}s_{jk}^2 & -2L_{jk}c_{jk}s_{jk} \\ -L_{ki}c_{ki}^2 & -L_{ki}s_{ki}^2 & -2L_{ki}c_{ki}s_{ki} \end{bmatrix} \tag{9}$$

where E, t, ν are the elasticity modulus, the thickness of the slab and the Poisson's ratio, respectively. The nodal forces vector is defined as:

$$\{P\} = [B]\{M\} \tag{10}$$

3.2 Lumped Damage Mechanic Approach

For the Lumped Damage Mechanics (LDM) approach, the inelastic effects (damage and plastic rotations) of the element are lumped in the sides (Fig. 1(c)). To define the damaged configuration, six extra variables are insert in the model, being the damage and plastic rotation variables for each side, as shown in (Fig. 1(d)). The damage variable d_{ij} and the plastic rotation ϕ_{ij}^p represent the concrete cracking and the reinforcement yielding along the hinge line *ij* and so for the other three sides. Considering the inelastic effects, the elasticity law are rewritten:

$$\{\Phi - \Phi^p\} = [F(D)]\{M\} \rightarrow [F(D)] = \begin{bmatrix} \frac{F_0[1,1]}{1-d_{ij}} & F_0[1,2] & F_0[1,3] \\ F_0[2,1] & \frac{F_0[2,2]}{1-d_{jk}} & F_0[2,3] \\ F_0[3,1] & F_0[3,2] & \frac{F_0[3,3]}{1-d_{ki}} \end{bmatrix} \tag{11}$$

The damage evolution laws are given by the Griffith criterion:

$$\begin{cases} \dot{d_{ij}} = 0 \rightarrow G_{ij} < R(d_{ij}) \\ G_{ij} = R(d_{ij}) \rightarrow \dot{d_{ij}} > 0 \end{cases} \tag{12}$$

$$G_{ij} = \frac{\partial W}{\partial d_{ij}} = \frac{(L_{ij}m_{ij})^2 F[1,1]}{2(1-d_{ij}^2)}$$

$$R_{ij} = R_{ij}^0 + q_{ij}\frac{ln(1-d_{ij})}{1-d_{ij}}$$

where R_{ij}^0 and q_{ij} are parameters of the model. Finally, the plastic evolution laws are given by:

$$\begin{cases} \dot{\phi_{ij}^p} = 0 \rightarrow f_{ij} < 0 \\ f_{ij} = 0 \rightarrow \dot{\phi_{ij}^p} > 0 \end{cases} \tag{13}$$

$$f_{ij} = \left| \frac{L_{ij}m_{ij}}{1-d_{ij}} - c_{p,ij}\phi_{ij}^p \right| - k_0^{ij}$$

where $c_{p,ij}$ and k_0^{ij} are parameters of the model. An advantage of the proposed model is that its parameters may be associated to the classical reinforced concrete theory parameters (cracking moment, plastic moment, ultimate moment and ultimate plastic rotation). For a detailed review see Florez-Lopez et al. [12] and Cunha et al. [19] .

4 Numerical applications

This section presents the results for three reinforced concrete slabs, experimentally tested by Sawczuk and Jaeger [6], under different boundary conditions and geometries, in which these authors did not present information on the bearing capacity of the slabs. Therefore, the numerical results were compared to the experimental and YLT ones, in terms of collapse load and the cracking pattern.

4.1 Retangular Reinforced Concrete Slab

The fist example is a rectangular RC slab under a concentrated load in its center load, which dimensions are 1.44 m x 2.16 m x 0.06 m, simply supported along all edges and fixed in the corners. The reinforcement was made of steel bars with a diameter of 4 mm, each 4 cm, for both directions. The distances between the center of gravity of

the reinforcement and the extreme compression fibers were 4.4 cm and 4.8 cm in X and Y directions, respectively, leading to reinforcement ratios were equal to 0.715% and 0.655%, in directions X e Y, respectively. The physical properties of the steel bars were yielding load, elasticity modulus, Poisson's ratio, and yielding strain equal to 304 MPa, 115.78 GPa, 0.3, and 4.45‰, respectively. The physical properties of the concrete were: compressive strength, elasticity modulus, and Poisson's ratio equal to 18.63 MPa, 15 GPa, and 0.2, respectively. The simulation was made considering the double symmetry of the slab, which mesh had 145 nodes and 64 finite elements. The numerical and experimental results are presented in Fig. 2, which visualization of the results were replicated for all slab.

Figure 2(a)-(b) presents the numerical results of damage and plastic rotation distribution. Note that the damage results are quite close to the cracking pattern observed experimentally (Fig. 2(c)), presenting the main cracking lines, in a "X" shape, and damaged regions parallels to the main crack. The plastic rotations also are in agreement with the collapse mechanism expected by the literature. Sawczuk and Jaeger [6] did not present the Force vs. Deflection curves. Fig. 2(d) presents the Load vs. Deflection results for the numerical model, which bearing capacity was equal to 46.78 kN, and by the YLT, equal to 50.07 kN, that results are close and the numerical one is in favor of the safety.

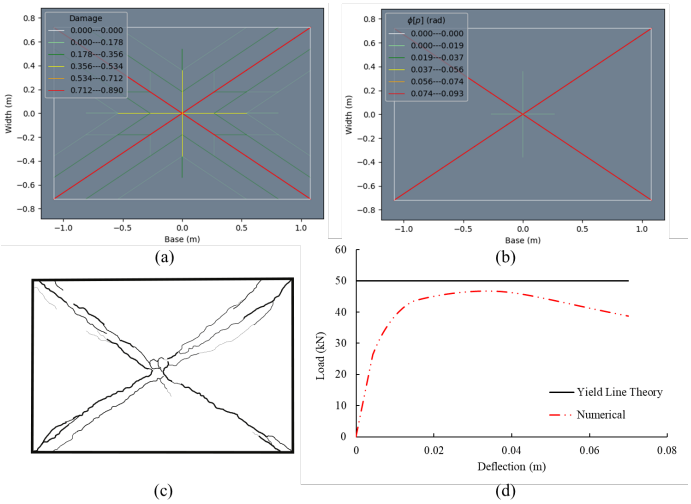

Figure 2. Rectangular slab: (a) damage condition, (b) Plastic rotations, (c) cracking pattern [6] and (d) Force vs. Deflection curve

4.2 Square Reinforced Concrete Slab

The second example is a square RC slabs with dimensions of 1.44 m x 1.44 m x 0.06 m, simply supported along all edges, which corners were fixed, and with a concentrated load in its center. The reinforcement arrangement was made using steel bars with diameter of 4.2 mm in the X direction and 4 mm in the Y direction, each 4 cm, for both directions. The distances between the center of gravity of the reinforcement bars and the extreme compression fibers were 4.38 cm and 4.8 cm, respectively, for the directions X and Y. Thus, the reinforcement ratios were equal to 0.79% and 0.66% in horizontal and vertical directions, respectively. Similar to the first example, it was considered the symmetry, and the mesh had 145 nodes and 64 finite elements, and the results were replicated for all slab. Likewise the first example, note that the results of cracking pattern observed experimentally (Fig 3(c)) is quite similar to the damaged configuration obtained numerically (Fig. 3(a)), with the main collapse mechanism in a "X" shape, corroborated by the plastic rotations, and damage lines parallel to the main one. The numerical Force vs. Deflection results are also quite close to the bearing capacity obtained by the YLT, equal to 43.06 kN and 47.23 kN, respectively, in favor of safety.

4.3 Asymmetric Square Reinforced Concrete Slab

The third example is an asymmetric slab, which three edges were simply supported, and the last one was free, with the corners fixed 4(a). The physical properties and geometric information of the slabs are equal to the second

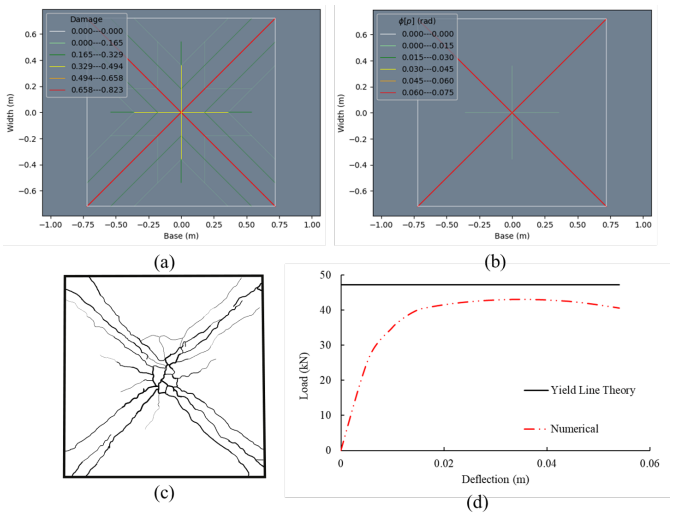

Figure 3. Square slab: (a) damage condition, (b) Plastic rotations, (c) cracking pattern [6] and (d) Force vs. Deflection curve

example. It was considered the vertical symmetry and the mesh had 281 nodes and 128 finite elements. Note that for this example, the simulations leaded to damage distribution that are in agreement with the experimental cracking pattern, as shown in Fig. 4(b) and (d). Note that, for this boundary conditions, the collapse mechanism is in "Y" shape, which is observed by the plastic rotations (Fig. 4(c)). The Force vs. Deflection curve for this slab is presented in Fig. 4(e), which bearing capacity of the slab was equal to 32.37 kN, while the value computed by the YLT was equal to 34.58 kN. These results corroborate the previous ones, which the complex cracking patterns were achieved by the numerical simulations and the bearing capacity of the slabs are close to the reference ones.

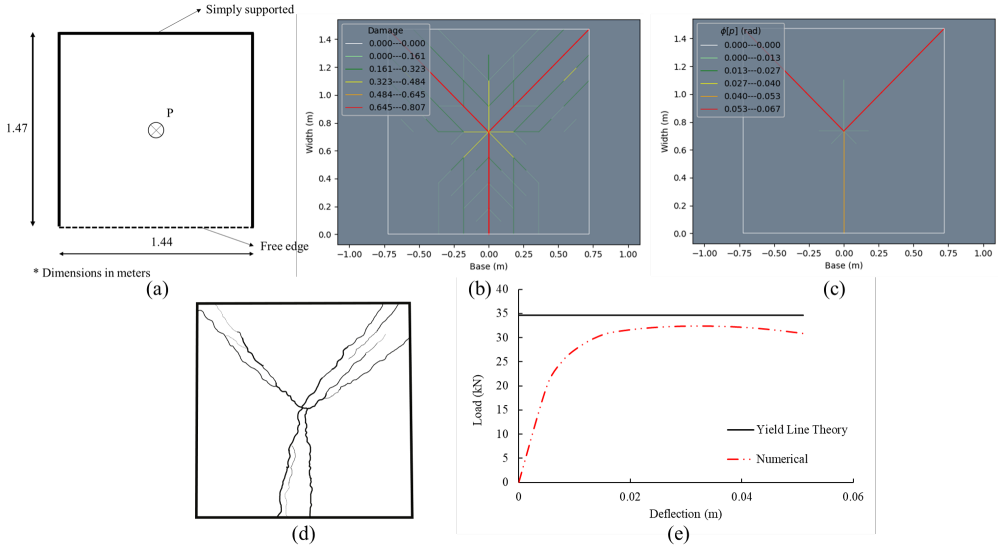

Figure 4. Asymmetric slab: (a) test set-up, (b) damage condition, (c) Plastic rotations, (d) cracking pattern [6] and (e) Force vs. Deflection curve

5 Conclusions

Lumped Damage Mechanics has been applied for several engineering problems and showing a high accuracy to describe the nonlinear problems. This paper presented the analysis of reinforced concrete slabs, by applying the LDM in the constant moment triangle. It was possible to note that the numerical damage distributions for all

cases are in agreement with the cracking pattern experimentally observed. The Load vs. Deflection results are also available, which bearing capacity of the slab were achieved quite close to the values that are computed by the yielding line theory.

Acknowledgements. The first author acknowledges CAPES (Coordenação de Aperfeiçoamento de Pessoal de Nível Superior) for his D.Sc. scholarship. The authors acknowledge the Graduate Program in Civil Engineering of the Federal University of Alagoas for the English proofreading of this paper.

Authorship statement. The authors hereby confirm that they are the sole liable persons responsible for the authorship of this work, and that all material that has been herein included as part of the present paper is either the property (and authorship) of the authors, or has the permission of the owners to be included here.

References

[1] C. Bach. *Versuche über die Widerstandsfähigkeit ebener Platten*. Springer, 1891.
[2] A. Nilson. *Design of concrete structures*. Number 12th Edition, 1997.
[3] Å. Ingerslev. The strength of rectangular slabs. *Struct. Eng*, vol. 1, n. 1, pp. 3–14, 1923.
[4] K. W. Johansen. *Brudlinieteorier*. I kommission hos J. Gjellerup, 1943.
[5] T. H. d. M. v. Langendonck. Teoria elementar das charneiras plásticas, 1970.
[6] A. Sawczuk and T. Jaeger. *Grenztragfähigkeits-Theorie der Platten*. Springer-Verlag, 1963.
[7] S. E. Grkem and M. H*ö*sem. Load capacity of high-strength reinforced concrete slabs by yield line theory. *Computers and Concrete*, vol. 12, n. 6, pp. 819–829, 2013.
[8] B. Sun and Z.-D. Xu. A continuum damage-based three-dimensional fracture simulation method for brittle-like materials. *International Journal of Damage Mechanics*, vol. 31, n. 4, pp. 508–531, 2022.
[9] A. R. V. Wolenski, A. B. Monteiro, S. S. Penna, R. L. d. S. Pitangueira, and F. B. Barros. Damage propagation using novel g/xfem strategies: computational aspects and numerical investigations. *Journal of the Brazilian Society of Mechanical Sciences and Engineering*, vol. 42, pp. 1–14, 2020.
[10] G. K. Singh, K. Patel, S. Chaudhary, and A. Nagpal. Methodology for rapid estimation of deflections in two-way reinforced concrete slabs considering cracking. *Practice Periodical on Structural Design and Construction*, vol. 26, n. 2, pp. 04021003, 2021.
[11] A. Cipollina, A. López-Inojosa, and J. Flórez-López. A simplified damage mechanics approach to nonlinear analysis of frames. *Computers & Structures*, vol. 54, n. 6, pp. 1113–1126, 1995.
[12] J. Florez-Lopez, M. E. Marante, and R. Picón. *Fracture and Damage Mechanics for Structural Engineering of Frames: State-of-the-Art Industrial Applications: State-of-the-Art Industrial Applications*. IGI global, 2014.
[13] J. A. Bazán, A. T. Beck, and J. Flórez-López. Random fatigue of plane frames via lumped damage mechanics. *Engineering Structures*, vol. 182, pp. 301–315, 2019.
[14] D. V. d. C. Teles, da R. N. Cunha, D. L. N. d. F. Amorim, R. Picon, and J. F. Lopez. Parametric study of dynamic behaviour of rc dual system design with the brazilian standard code using the lumped damage model. *Journal of the Brazilian Society of Mechanical Sciences and Engineering*, vol. 43, n. 5, pp. 246, 2021.
[15] R. M. Bosse, J. Flórez-López, G. M. Gidrão, I. D. Rodrigues, and A. T. Beck. Collapse mechanisms and fragility curves based on lumped damage mechanics for rc frames subjected to earthquakes. *Engineering Structures*, vol. 311, pp. 118115, 2024.
[16] D. L. Amorim, D. P. Neto, S. P. Proença, and J. Flórez-López. The extended lumped damage mechanics: A new formulation for the analysis of softening with fe size-independence. *Mechanics Research Communications*, vol. 91, pp. 13–18, 2018.
[17] R. A. Picón, D. M. Santos, D. V. Teles, D. L. Amorim, X. Zhou, Y. Bai, S. P. Proenca, and J. Florez-Lopez. Modeling of localization using nash variational formulations: The extended damage mechanics. *Engineering Fracture Mechanics*, vol. 258, pp. 108083, 2021.
[18] D. V. Teles, R. N. Cunha, R. A. Picon, D. L. Amorim, Y. Bai, S. P. Proenca, and J. Florez-Lopez. A new formulation of cracking in concrete structures based on lumped damage mechanics. *Structural Engineering and Mechanics*, vol. 88, n. 5, pp. 451–462, 2023.
[19] R. N. Cunha, D. L. Amorim, S. P. Proença, and J. Flórez-López. Modeling the initiation and propagation of complex networks of cracks in reinforced concrete plates. *Engineering Structures*, vol. 308, pp. 117993, 2024.
[20] Y. Toi and K. Hasegawa. Element-size independent, elasto-plastic damage analysis of framed structures using the adaptively shifted integration technique. *Computers & structures*, vol. 89, n. 23-24, pp. 2162–2168, 2011.
[21] L. Morley. The constant-moment plate-bending element. *Journal of Strain Analysis*, vol. 6, n. 1, pp. 20–24, 1971.